Zoology 157 (2023) 126078

Contents lists available at ScienceDirect

Zoology

journal homepage: www.elsevier.com/locate/zool

Get to the point: Claw morphology impacts frictional interactions on rough substrates

Alexandra M. Pamfilie [b,1], Austin M. Garner [a,b,*,2], Anthony P. Russell [c], Ali Dhinojwala [a,d], Peter H. Niewiarowski [a,b]

[a] Integrated Bioscience Program, The University of Akron, Akron OH 44325–3908, USA
[b] Department of Biology, The University of Akron, Akron OH 44325–3908, USA
[c] Department of Biological Sciences, University of Calgary, Calgary, AB T2N 1N4, Canada
[d] Department of Polymer Science, The University of Akron, Akron, OH 44325–3909, USA

ARTICLE INFO

Keywords:
Function
Morphometrics
Anolis
Biomechanics
Surface topography

ABSTRACT

Claws are a common anatomical feature among limbed amniotes and contribute to a variety of functions including prey capture, locomotion, and attachment. Previous studies of both avian and non-avian reptiles have found correlations between habitat use and claw morphology, suggesting that variation in claw shape permits effective functioning in different microhabitats. How, or if, claw morphology influences attachment performance, particularly in isolation from the rest of the digit, has received little attention. To examine the effects of claw shape on frictional interactions, we isolated the claws of preserved specimens of Cuban knight anoles (*Anolis equestris*), quantified variation in claw morphology via geometric morphometrics, and measured friction on four different substrates that varied in surface roughness. We found that multiple aspects of claw shape influence frictional interactions, but only on substrates for which asperities are large enough to permit mechanical interlocking with the claw. On such substrates, the diameter of the claw's tip is the most important predictor of friction, with narrower claw tips inducing greater frictional interactions than wider ones. We also found that claw curvature, length, and depth influence friction, but that these relationships depend on the substrate's surface roughness. Our findings suggest that although claw shape plays a critical role in the effective clinging ability of lizards, its relative importance is dependent upon the substrate. Description of mechanical function, as well as ecological function, is critical for a holistic understanding of claw shape variation.

1. Introduction

Claws are present in all classes of limbed amniotes and perform a multitude of functions, including attachment, locomotion, and prey capture (Feduccia, 1993; Thomson and Motani, 2021; Zani, 2000). Claw shape is highly variable across taxa yet appears to be tightly linked with habitat use. Climbing birds and lizards, for example, often possess claws that are more tightly curved and hook-like, while those of terrestrial species are relatively long and straighter (Crandell et al., 2014; D'Amore et al., 2018; Falvey et al., 2020; Feduccia, 1993; Teixeira-Filho et al., 2001; Thomson and Motani, 2021; Tulli et al., 2009; Yuan et al., 2019). The claws of small arboreal lizards are generally used during locomotion and attachment, suggesting that ecomorphological variation in claw shape has functional significance and that this variation is related to success in particular microhabitats.

Claws induce attachment forces primarily through mechanical interlocking with surface asperities or particles, although claws are also capable of inducing considerable friction when interlocking is not possible (Dai et al., 2002). If the depressions between substrate asperities are sufficiently wide and deep relative to the claw tip and its degree of taper, mechanical interlocking can occur, and claws can subsequently induce substantial clinging forces. Indeed, measurement of clinging forces in live animals with and without the presence of claws demonstrates the critical role of the claw in clinging to rough substrates (Bullock and Federle, 2011; Naylor and Higham, 2019; Pattrick et al., 2018; Scholz et al., 2010). Regardless of surface roughness, claws may

* Correspondence to: Department of Biology & BioInspired Institute, Syracuse University, Syracuse, NY 13244 USA.
E-mail address: agarner@syr.edu (A.M. Garner).
[1] Present address: Department of Ecology and Evolution, Stony Brook University, Stony Brook, NY 11794–5245, USA
[2] Present address: Department of Biology & BioInspired Institute, Syracuse University, Syracuse, NY 13244, USA

https://doi.org/10.1016/j.zool.2023.126078
Received 1 August 2022; Received in revised form 30 January 2023; Accepted 18 February 2023
Available online 20 February 2023

also mechanically interlock with soft surfaces through perforation or indentation (Thomson and Motani, 2021).

Interestingly, few studies have directly investigated how claw morphology impacts clinging performance. Zani (2000) measured clinging abilities and digital morphology across lizards and found significant positive relationships between claw curvature (derived from the opening angle of the claw) and clinging force on a smooth acrylic substrate, as well as between claw height (here, described as depth) and clinging force on two rough substrates. Zani (2000) used several species of lizard that possess both claws and adhesive toe pads, making it difficult to ascertain whether claw shape was directly influencing clinging ability via frictional interactions or if it was indirectly affecting performance of the adhesive pad. This is particularly apparent in the unexpected positive relationship between claw curvature and clinging performance on a smooth substrate. Claws are unlikely to improve clinging performance directly on smooth substrates like acrylic because surface asperities are much too small to promote mechanical interlocking or increased frictional interactions. Adhesive toe pads, on the other hand, carry hair-like filaments (setae) that promote intermolecular adhesion by making intimate contact with the substrate and are thought to perform best on smooth substrates (Autumn and Peattie, 2002; Maderson, 1964; Russell and Johnson, 2007; Russell and Johnson, 2014). Some authors have suggested that increases in claw curvature may lead to setae making better contact with the surface (i.e., greater contact fraction), thereby increasing intermolecular interactions and, subsequently, clinging ability (Garner et al., 2017). Recent studies, however, measured clinging ability before and after experimental debilitation of claws and found that claw removal had no significant impact on clinging ability on smooth substrates (Bullock and Federle, 2011; Garner et al., 2017; Naylor and Higham, 2019). Therefore, the functional significance of claw curvature to clinging on smooth substrates is unclear. Furthermore, although one other study measuring clinging ability of lizards without adhesive toe pads corroborated Zani's (2000) observations of claw depth scaling positively with clinging ability (Tulli et al., 2012), no experiment has examined the relationship between claw form and function in isolation from the rest of the digit.

Theoretically, greater claw curvature, or greater opening angles of the claw, should increase friction on a rough substrate by redirecting force onto the face of surface asperities, inducing mechanical interlocking (Cartmill, 1985; Yuan et al., 2019). Claws are manipulated via the digital extensor and flexor musculotendinous system; thus, tendon attachment sites may also influence the claw's interaction with the substrate (e.g., the angle of attack) (Fig. 1). The digital extensor tendon attaches to the dorsally situated extensor tubercle of the ungual phalanx, while the digital flexor tendon attaches to its ventrally situated flexor tubercle. The ungual phalanx of deep claws, like those of many arboreal species, generally articulates with the penultimate phalanx such that its articular facet is offset dorsally (e.g., *Gekko gecko*; Russell, 1975), indicating that the in-lever arm for flexion is relatively longer than that for extension. Therefore, deeper claws should be capable of inducing greater forces on the substrate during flexion (via increased mechanical advantage) and swifter movement of the claw during extension than relatively shallower claws (Cartmill, 1985; Thomson and Motani, 2021).

Friction forces induced by claws should also be impacted by variation in surface roughness and this should interact with the morphology of the claw tip. Previous work posits that claw tips with diameters wider than that of surface asperities should be less likely to mechanically interlock and generate appreciable attachment forces (Dai et al., 2002). However, claws gain purchase by penetrating the depressions between asperities, thus the shape and dimensions of the surface depressions are much more likely to be important factors for mechanical interlocking than simply the height of asperities (Scholz et al., 2010). Claw tips with smaller diameters and more attenuated tapering will be able to penetrate smaller surface depressions, but will be at greater risk of breakage (Asbeck et al., 2006; Pattrick et al., 2018). Additionally, it has not been investigated if two claws with identical lengths but differences in depth possess different bending stiffnesses. Deeper claws will be stiffer than shallow claws, and this could influence interactions with the substrate.

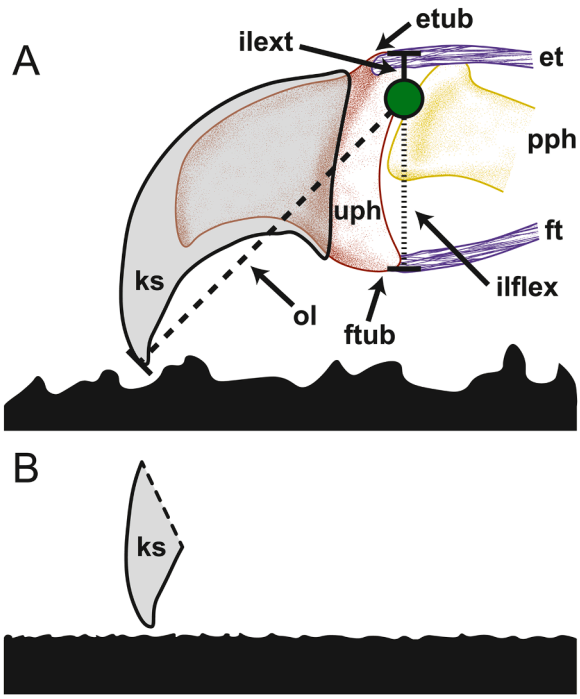

Fig. 1. Anatomical sketch of the claw-based attachment system of squamates and how it interacts with the substrate. This figure uses an *Anolis equestris* claw as an example of a typical claw shape in small arboreal squamates. (A) The penultimate phalanx (pph) of the digit articulates with the ungual phalanx (uph), which composes the bony core of the claw. The bony core is covered in a keratin sheath (ks) that interacts with the external environment. The claw's position (e.g., angle of attack) is controlled via the flexor-extensor musculotendinous system. The extensor tendon (et) attaches to the dorsally situated extensor tubercle (etub) of the ungual phalanx, while the flexor tendon attaches to the more ventrally situated flexor tubercle (ftub) of the ungual phalanx. The articulatory facet between the penultimate and ungual phalanges is generally offset dorsally in arboreal lizards (e.g., *Gekko gecko*; Russell, 1975), creating a relatively longer in-lever arm for the flexor tendon (ilflex) compared to that for the extensor tendon (ilext). Given a constant out-lever (ol), this geometry likely results in greater force induction during flexion and swifter retraction of the claw during extension. The claw is depicted as approaching a substrate with asperities that are much wider and taller than the diameter of the claw's tip, a situation predicted to permit effective mechanical interlocking. (B) The tip of the same claw as pictured in (A) is depicted but approaching a substrate with asperities that are much narrower and shorter than the diameter of the claw tip. In this case, mechanical interlocking is likely not possible, thus attachment force will result solely from frictional interactions with the substrate.

Studying the frictional performance of claws isolated from the rest of the digit also provides the opportunity to manipulate the claw in ways that would be otherwise impossible in live specimens. Mechanical alteration of the keratin sheath of claws, for example, allows for manipulation of tip shape, distribution of material along the proximodistal axis of the claw, and other dimensional properties. Furthermore, such alterations permit the examination of function of morphologies beyond those observed in nature.

Here we examine the relationships between claw morphology and performance using the claws of the Cuban knight anole (*Anolis equestris*) in isolation from the rest of the animal. We use geometric morphometric methods to quantify the shape variation in both unmodified and reshaped claws and compare this to variation in friction force induction on surfaces with different roughness profiles. We also analyze claw morphology *sensu* Zani (2000) to critically assess and directly compare our qualitative results to previous work and findings. We predicted that

claws with relatively tighter curvature, deeper bases (or greater height), and relatively shorter length will induce the greatest friction forces on rough surfaces as long as the diameter of the claw tip is less than the width of surface depressions.

2. Methods

2.1. Animal and sample preparation

The terminal portions of the digits (distal to the toe pad; Fig. 2a, SI Tables 1 and 2) of five alcohol-preserved Cuban knight anole (*Anolis equestris*, Merrem, 1820) specimens were removed and affixed with epoxy (Loctite Epoxy Instant Mix; Henkel Corporation, Westlake, OH USA) to glass slides such that the claw tip was approximately perpendicular to the slide (Fig. 2b). Animals were used for a prior study (Garner et al., 2021) where they were fixed with 10% neutral-buffered formalin following euthanasia and stored in 70% ethanol. Because all five specimens were preserved in the same way at the same time, any effects of preservation on the claws' material properties should be identical across individuals. The epoxy was allowed to cure for at least 24 h. The mounted specimens were then trimmed of excess proximal tissue as necessary, such that only the distalmost part of the penultimate phalanx and the claw remained (Fig. 2b).

Twenty claws (n = 20; SI Table 1; hereafter referred to as the main sample) were employed in the investigation of how claw shape impacts friction force generation on substrates of varying surface roughness. These claws were sampled from digits II, III, and V of the pes of four of the five individuals. We did not sample digit I because its orientation is different from that of the other digits, which may have had a confounding effect on its shape and force induction. Digit IV was not included because of its use in a previous study (Garner et al., 2021). We ensured that only one claw (either right or left) was modified (see SI Table 1) for each digit per individual.

Half of the twenty claws (n = 10) were reserved for testing in their unmodified state, whereas the remaining half (n = 10) underwent shape modification using a rotary tool (Dremel Moto-Tool Model 395 Type 3; Dremel, Racine, WI, USA). During the modification process, the claw was already adhered to the glass slide and was held in place on a steady surface while the rotary tool was moved around the claw. Modification included removing claw material from any combination of the inner curve, outer curve, or tip of the claw, followed by reshaping to maintain a pointed tip (SI Table 1). A single researcher modified all claws in one session to ensure that described changes were consistent and relative to one another (e.g., "shortened" vs. "slightly shortened"). One "replicate" of each combination of these modifications was included because the number of combinations of modifications were limited. For example, two claws had their inner curves modified (followed by extra reshaping to maintain overall claw shape), two claws had their outer curves modified, and so on (SI Table 2). These are not true replicates, however, because the precision necessary to achieve this was not possible with the rotary tool. We visually verified that the desired shape change was occurring and were cautious to not remove too much material that would otherwise undermine the structural integrity of the claws. This procedure provided us with the opportunity to analyze claw shapes not naturally present in our sample.

To confirm the integrity of claws used in our main sample we employed a different set of claws (n = 15, SI Table 2; hereafter referred to as the wear sample) from the same specimens and tested them

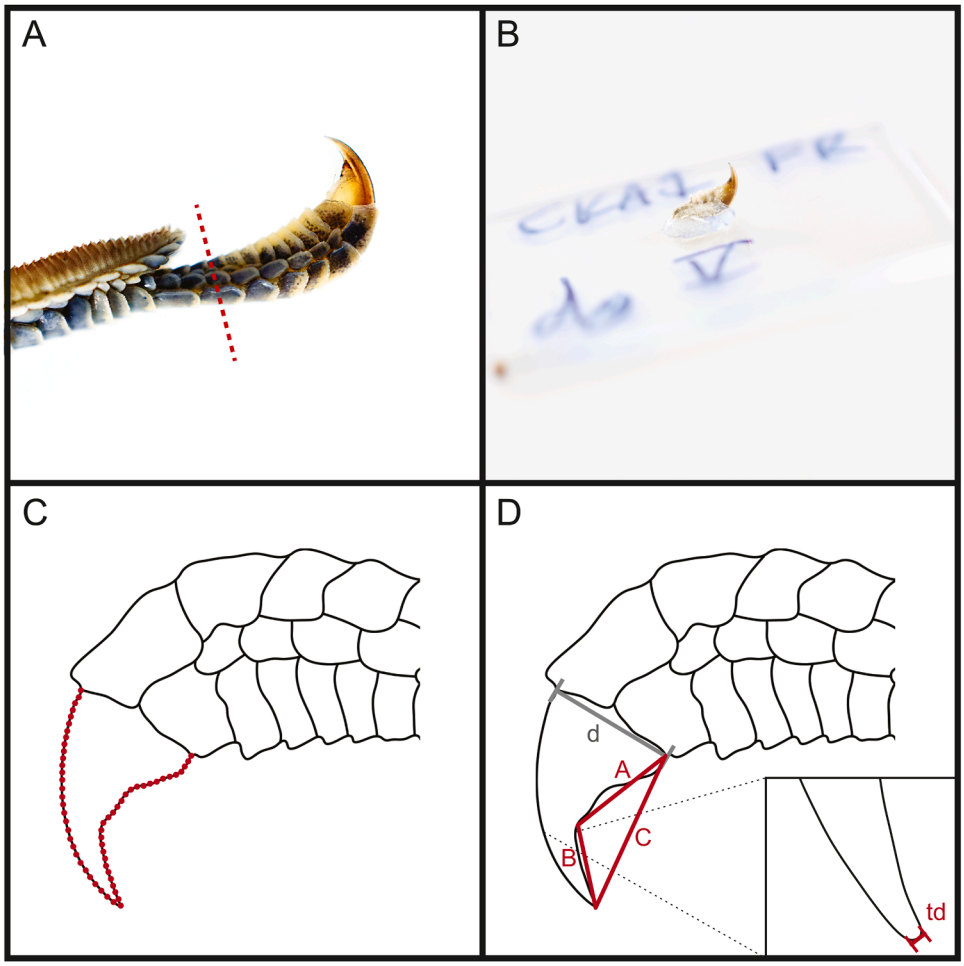

Fig. 2. Preparation and morphometric measurement of the isolated claws of *Anolis equestris*. (A) Toe pad (to the left) and claw of *Anolis equestris*. The red dashed line represents the plane at which the distal end of the digit was removed. (B) Following inverted attachment of the specimen to a glass slide via epoxy, the specimen was trimmed, if necessary, so that only the distalmost part of the penultimate phalanx and the claw remained. (C) Placement of 60 semilandmarks along the claw's outline in lateral view (Tinius and Russell, 2017). (D) A triangle fitted to the claw's inner curve, *sensu* Zani (2000). Claw length is the sum of lengths *A* and *B*, which meet at the inflection point of the ventral curve. Claw curvature is calculated from the three line segments of the depicted triangle via Eq. 5. Claw depth is marked as *d*. We also measured claw tip diameter (td), defined as the length of the flattened segment connecting the dorsal and ventral curves of the claw.

repeatedly on two of the substrates. This was done to examine if, or how, the claws experienced wear between trials and if this had any influence on maximum friction force. These claws were selected from the manus of all five specimens. In this case, digits I and III were excluded because of potential confounding effects and use in preliminary testing, respectively. Digit IV of the right manus was excluded because of use in a previous study (Garner et al., 2021). We exclusively used the pes in the main sample and the manus in the wear sample to minimize any potential for confounding differences in shape or material properties between these autopodia. In cases where we were able to sample the same digit from both manūs of an individual, these were assigned to different sandpapers. Claws of the wear sample were prepared in the same way as described above but were left unmodified.

2.2. Profilometry procedure and substrate analysis

Four different substrates were used in this study: glass, 1500-grit sandpaper, 800-grit sandpaper, and 320-grit sandpaper (3M Wetordry Sandpaper; 3 M, St. Paul, MN, USA). Glass was employed as the smooth, low friction substrate against which frictional performance on substrates of increasing roughness could be assessed. These sandpapers were selected for the apparent range of surface qualities they would possess, with 1500-grit sandpaper representing a surface with asperities likely too small for most claws to interlock with, 320-grit sandpaper representing a surface with asperities with which interlocking could occur, and 800-grit sandpaper representing an intermediate case. To gain a better understanding of the substrates' roughness profiles, a sample of each was examined with a stylus profilometer (Bruker DektakXT; Bruker, Tucson, AZ, USA). Three separate line scans, each 1 mm in length, were taken of each sandpaper substrate to collect a surface profile. Three separate line scans were also taken on glass, each 200 μm in length. Four surface roughness parameters were calculated from the line scans: arithmetic mean height (R_a), root mean square (RMS) height (R_q), RMS slope ($R_{\Delta q}$), and mean width between asperities (R_{sm}). R_a and R_q are descriptors of mean height deviation and were calculated via Eqs. 1 and 2, respectively. $R_{\Delta q}$ is a descriptor of the mean slope of asperities and was calculated via Eq. 3. R_{sm} is a descriptor of the spacing between asperities and was calculated via Eq. 4.

$$R_a = \frac{1}{L}\int_0^L |y(x)dx| \tag{1}$$

$$R_q = \sqrt{\frac{1}{L}\int_0^L y^2(x)dx} \tag{2}$$

$$R_{\Delta q} = \sqrt{\frac{1}{L}\int_0^L \left[\frac{dy(x)}{dx}\right]^2 dx} \tag{3}$$

$$R_{sm} = \frac{1}{m}\sum_{i=1}^{m} Xs_i \tag{4}$$

Where they occur in Eqs. 1–4, L equals the profile length (1 mm or 200 μm, in our study), y is equivalent to the profile height at position x along L, m is the total number of asperities in the line scan, and X_{si} is the distance between asperities. In Eq. 4, an asperity is defined as the element of the profile between two consecutive crossings of the mean profile height. The distance between asperities (X_{si}) is calculated as the linear length between two subsequent vertical crossings of the mean profile height. Roughness parameters were calculated for each line scan using Eqs. 1–4 and the values averaged to obtain mean roughness parameters (Table 1).

Table 1
Mean arithmetic mean height (R_a), root mean square (RMS) height (R_q), RMS slope ($R_{\Delta q}$), and mean spacing between asperities (R_{sm}) of the four tested substrates. Values are means ± 1 standard error. Measurements of the three sandpapers are derived from 1 mm scans; the glass (*) measurements are derived from 200 μm scans.

Substrate	R_a (μm)	R_q (μm)	$R_{\Delta q}$	R_{sm} (μm)
Glass*	$1.0 * 10^{-3} \pm 4.0 * 10^{-4}$	$3.0 * 10^{-3} \pm 1.0 * 10^{-3}$	$5.0 * 10^{-3} \pm 1.0 * 10^{-3}$	2.33 ± 1.00
1500-grit Sandpaper	4.01 ± 0.47	5.04 ± 0.54	0.6 ± 0.02	55.74 ± 3.91
800-grit Sandpaper	4.01 ± 0.33	5.19 ± 0.28	0.38 ± 0.02	101.71 ± 14.36
320-grit Sandpaper	12.10 ± 2.79	14.70 ± 3.13	0.82 ± 0.07	124.38 ± 27.08

2.3. Friction measurements

To measure friction, claws were displaced along the substrates while affixed to a friction cell employing two picomotors (Newport NewFocus Picomotors; Newport Corporation, Irvine, CA, USA) that finely manipulated the relative positions of the substrate and claw. When the substrate and claw come into contact, forces are exerted on springs that change the relative positions of attached capacitors. Measured changes in capacitance correspond to changes in applied normal and friction forces, as determined via calibration with a series of small weights. For testing, claws were brought into contact with the substrate with preloads of 39.1 ± 4.8 mN. The distance between the glass slide bearing the claw and the substrate that generated this preload was maintained throughout the trial. To determine the appropriate preload, the average antemortem mass of the *A. equestris* specimens was calculated and divided by 20, yielding the approximate loading on one of the animal's digits. The claw was brought into contact perpendicular to the substrate. This could differ from the way the claw is placed by the animal, where it may come into contact at an angle that can be actively modulated via the musculotendinous system (Bloch and Irschick, 2005; Garner et al., 2017). That angle is unknown (and likely variable), hence our choice of a perpendicular approach. Once contact was made, the claw was displaced 1 mm across the substrate, simulating the animal retracting the limb towards its body. Friction and normal forces were measured throughout the displacement. From these data, maximum friction force, average peak friction force, initial normal (preload) force, and average normal force were calculated in millinewtons for each trial. Average peak friction force was found using the Scipy *find_peaks* function in Python (Virtanen et al., 2020).

The above procedure was repeated four times (once on each of the four substrates) for each claw in the main sample (SI Table 1). The order of substrates was randomized via a nonrepeating random number generator. For the wear sample (SI Table 2), the above procedure was repeated five times for each claw on either the 1500-grit sandpaper (n = 8) or the 320-grit sandpaper (n = 7). These two substrates represented the smoothest and roughest sandpapers, respectively. This was done to examine the amount of change in shape, if any, taking place between trials, if this varied among sandpapers, and if any change in shape had a significant impact on maximum friction force.

2.4. Morphometric analysis

A lateral image of each claw was taken prior to every trial via a light microscope (Olympus SZX16 Stereomicroscope, Olympus Corporation, Shinjuku, Tokyo, Japan) and matched to the corresponding force data. Each claw was imaged prior to each trial; claws in the main sample were imaged four times (once for each substrate) and claws in the wear sample were imaged five times (once for each trial). This repeated imaging ensured that the shape of the claw was accurately documented prior to force induction. In the wear sample, we found generally non-

significant effects of claw wear across repeated trials on shape and friction (see SI Tables 3 and 4 for full results).

Past studies have used a variety of methods for approximating and describing the features of claws. Tinius and Russell (2017) found that a geometric morphometric approach represents claw shape accurately without approximating the claw to any particular shape. Because of its ability to represent the holistic shapes of claws, their methodology was adopted here with modifications. On the photographic image of each claw in lateral view, 60 semilandmarks were placed along its outline in tpsdig2 (Rohlf, 2018), 30 semilandmarks along the outer curve, and 30 along the inner curve, with the first and sixtieth semilandmarks placed, respectively, at the dorsal and ventral emergences of the claw sheath, and the thirtieth semilandmark placed at the tip (Fig. 2c) (Tinius and Russell, 2017). Semilandmark information was imported into R via .tps file where subsequent shape analyses (i.e., generalized Procrustes analysis, principal component analysis) were achieved via the *geomorph* package (Adams et al., 2017). During Procrustes superimposition, semilandmarks were allowed to slide along the curve to better approximate the shape of the claw; full thin plate spline (TPS) mapping was used to estimate bending energy of the splines (Gunz and Mitteroecker, 2013).

To verify our results in the context of others' findings, we also quantified claw morphology using Zani's (2000) methodology, which fits a triangle to the inner curve of the claw (Tinius and Russell, 2017). The vertices of this triangle are located at the base of the claw, the tip of the claw, and the inflection point of the inner curve (Fig. 2d). From this triangle, measurements of length and curvature are derived (Zani, 2000). Claw length is the sum of the straight-line distances from the ventral emergence of the claw to the ventral curve's inflection point and from the inflection point to the claw tip (lengths A and B in Fig. 2d). Claw curvature is defined as the degrees of arc included in a circle fit to the triangle (Tinius and Russell, 2017; Zani, 2000). The formula for curvature is

$$Curvature = \frac{180}{\pi} * 2 * arcsine\left(\frac{\sqrt{\left(2{*}A^2 * B^2\right) + \left(2 * A^2 * C^2\right) + \left(2 * B^2 * C^2\right) - A^4 - B^4 - C^4}}{2AB}\right) \quad (5)$$

as described by Zani (2000). A claw with a high curvature value has a large opening angle and vice versa. In addition, claw depth is measured as the distance from the ventral emergence to the dorsal emergence of the keratinous claw sheath. The diameter of the claw tip has not been previously examined in relation to frictional performance, thus we also measured this parameter, defined as the length of the flattened segment connecting the dorsal and ventral curves of the claw. These measurements were taken using ImageJ (National Institutes of Health, Bethesda, MD).

2.5. Statistical analyses

Three principal component analyses (PCAs) were used to quantify shape across both samples. In all three PCAs, the significant PC axes were determined with the broken stick criterion via the *brokenStick* command in the R package *PCDimension* (Wang et al., 2018).

For the main sample (unmodified and modified claws), significant PC axes (generated via *geomorph* on covariances) were regressed against maximum friction force and average peak friction force as a function of substrate using linear regression. Because trends in the data were similar between maximum and average peak friction force, only maximum friction force is discussed here. Average peak friction force results are reported in SI Table 5. The significant PC axes were also regressed against claw tip diameter (SI Fig. 2) to examine whether the geometric morphometric approach indirectly captures variation in claw tip diameter. To account for any confounding variables, the specimen, the side of the body, and the digit each sample came from, as well as the trial and whether the claw was modified, were examined for relationships with maximum friction force with a multi-way ANOVA using JMP Pro 14 (SAS Institute, Inc.; Cary, NC USA). In this analysis, maximum friction force was the response variable for the predictor variables: specimen, side of the body, digit, trial, and whether it was modified. In addition, to check for an effect of claw size on shape, the Procrustes coordinates were regressed against centroid size via linear regression. Claw shape varied significantly with size (F=4.68, $p = 0.006$), thus we produced size-corrected claw shapes by obtaining the residuals from the linear regression of Procrustes coordinates versus centroid size and adding the consensus shape to those residuals (Klingenberg, 2016).

Also for the main sample, a second PCA (generated on correlations) was used to analyze the effects of univariate claw characters (length, depth, and curvature) on maximum friction force to replicate the methodology used in previous work (Zani, 2000). Three PC axes were identified, but only the first two met the broken stick criterion (Wang et al., 2018). Thus, we used the first two PC axes for subsequent analysis. Maximum friction force as a function of each PC was examined via series of linear regressions, similar to the PCs generated from the geometric morphometric results.

A third PCA (generated on covariances) quantified multivariate shape variation in the wear sample via the geometric morphometric methods described above. There was an effect of size in this analysis as well (F=12.65, $p < 0.001$); we again produced size-corrected shapes as above (Klingenberg, 2016). The first three PC axes accounted for 93.1% of the variation (SI Table 3), yet none of these met the broken stick criterion. Instead, we selected all PCs that accounted for more than 5% of the overall shape variation. Four repeated measures MANOVAs were implemented in JMP to analyze changes in each of the three PC axes and maximum friction force across trial number as a function of substrate. These evaluated if shape changes with trial, whether that change varied with substrate, and if there was any impact of force. Once corrected for size, there were no significant effects except for the effect of substrate on maximum friction force; full results are shown in SI Table 4.

3. Results

3.1. Surface roughness

Surface roughness parameters were calculated from surface profiles obtained via stylus profilometry and are displayed for each of four test substrates in Table 1. Arithmetic mean height (R_a) and root mean square (RMS) height (R_q) of glass were approximately 3–4 orders of magnitude lower than those of all sandpaper substrates. R_a and R_q of 320-grit sandpaper were approximately three times greater than those of the 1500-grit and 800-grit sandpapers, both of which had very similar R_a and R_q. RMS slope ($R_{\Delta q}$) of glass was the lowest of all substrates and was approximately two orders of magnitude lower than the sandpaper substrates. $R_{\Delta q}$ of the three sandpaper substrates varied considerably between them, with 320-grit sandpaper having the greatest $R_{\Delta q}$, followed by 1500-grit sandpaper, and then 800-grit sandpaper with the second lowest $R_{\Delta q}$ of all substrates. Mean spacing between asperities (R_{sm}) of glass was the lowest of all substrates and was approximately 1–2 orders

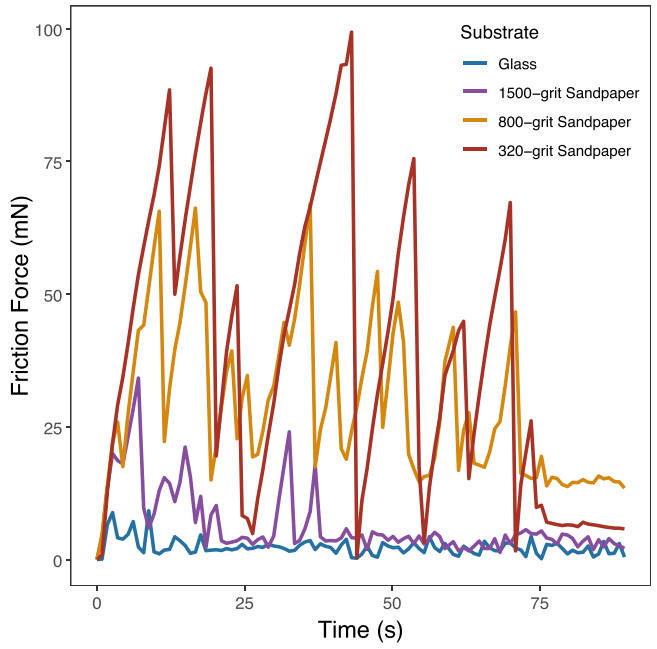

Fig. 3. Friction induced by claws displaced 1 mm along substrates of varying surface roughness. Representative traces of friction measured over time during a typical trial on each of the four substrates: glass, 1500-grit sandpaper, 800-grit sandpaper, and 320-grit sandpaper. Peaks in force may represent the claw interlocking with asperities in the surface, and valleys may correspond to slippage and subsequent interlocking with another asperity. However, this observation could not be confirmed given the small size of the *Anolis equestris* claws used in this study.

of magnitude lower than the sandpaper substrates. R_{sm} of the sandpaper substrates varied with grit size, with 320-grit sandpaper having the largest R_{sm}, followed by 800-grit sandpaper, and then 1500-grit sandpaper. Typical friction curves as a function of time and substrate are shown in Fig. 3.

3.2. Influence of claw shape on friction forces (geometric morphometrics – GM)

The PCA using geometric morphometric results from the main sample returned seventy-nine principal components (PCs), but as determined by the broken stick analysis, only the first four PCs explained significant variation in shape. Each of these accounted for more than 5% of the overall variance in shape (Table 2). The consensus shape with corresponding sample variance can be found in the supplementary information (SI Fig. 1).

Principal component 1 (GM PC1) primarily explained variation in claw length and depth, with smaller values representing relatively longer, shallower claws with highly tapered tips and higher values representing relatively shorter, deeper claws with less tapered tips (Fig. 4a). GM PC1 did not predict maximum friction force on glass ($p = 0.92$), 1500-grit sandpaper ($p = 0.79$), or 320-grit sandpaper ($p = 0.16$) but had an inverse relationship with maximum friction force on 800-grit sandpaper ($p < 0.001$; Table 3). Principal component 2 (GM PC2) primarily described variation in claw length and degree of tapering, with minimum values representing long, highly tapered claws that are shallow along much of their length and maximum values representing short, less tapered claws that are deep along much of their length (Fig. 4b). This principal component did not predict maximum friction force induction on any substrate ($p = 0.25$ for glass; $p = 0.36$ for 1500-grit sandpaper; $p = 0.45$ for 800-grit sandpaper; $p = 0.40$ for 320-grit sandpaper; Table 3). Principal component 3 (GM PC3) primarily described claws that exhibited large opening angles of the ventral curve at minimum values and small opening angles of the ventral curve at maximum values (Fig. 4c). While GM PC3 did not predict friction force on glass ($p = 0.63$), 1500-grit sandpaper ($p = 0.29$), or 800-grit sandpaper ($p = 0.31$), it did positively correlate with maximum friction force on 320-grit sandpaper ($p < 0.001$; Table 3). Principal component 4's (GM PC4) minimum values described uniformly tapered claws, whose dorsal and ventral curves form a triangle-like shape. The maximum values of GM PC4 represented deep claws, whose tips point more ventrally, rather than distally (Fig. 4d). Like GM PC2, this principal component did not significantly predict maximum friction force on any substrate ($p = 0.25$ for glass; $p = 0.58$ for 1500-grit sandpaper; $p = 0.67$ for 800-grit sandpaper; $p = 0.67$ for 320-grit sandpaper; Table 3).

To check for potential confounding variables within the main sample, characteristics of the samples were analyzed for trends. Maximum friction force was not predicted by the individual (F=0.56, d.f.=3, $p = 0.64$), side of the body ($t = 0.29$, d.f.=1, $p = 0.59$), or digit (F=0.27, d.f.=2, $p = 0.77$) from which the claw originated. Trial, as an indicator of how many times the specimen had already undergone testing, did not significantly predict maximum friction force (F=0.34, d.f.=3, $p = 0.80$). Interestingly, whether the claw's shape had been manipulated also did not significantly impact maximum friction force ($t = 1.89$, d.f.=1, $p = 0.17$).

3.3. Comparison to previous findings – Zani's (2000) methodology (univariate measures – UM)

In the main sample, the first two principal components cumulatively explained approximately 88% of the variation in claw shape as represented by Zani's (2000) methodology (Table 4; SI Table 7). The loadings of the measured univariate traits on the three principal components are shown in Table 5. Principal component 1 (UM PC1) largely explained variation in claw depth and length, both of which increased with increasing values of UM PC1. Maximum friction force did not vary significantly with UM PC1 on glass ($p = 0.71$), 1500-grit sandpaper ($p = 0.28$), or 800-grit sandpaper ($p = 0.63$) but varied significantly and positively with UM PC1 on 320-grit sandpaper ($p = 0.03$; Fig. 5a). UM PC2 generally explained variation in claw curvature, which increased with increasing values of UM PC2. Maximum friction force did not vary significantly with UM PC2 on any of the substrates (glass: $p = 0.30$; 1500-grit sandpaper: $p = 0.92$; 800-grit sandpaper: $p = 0.14$; 320-grit sandpaper: $p = 0.90$; Fig. 5b).

Table 2
The first four principal components of the PCA describing variation in claw shape in *Anolis equestris* as measured by semilandmarks (geometric morphometric [GM] data). This PCA was run on data from the main sample, comprising unmodified and modified (shape manually altered with rotary tool) claws. Some claws were modified to sample a greater variety of potential claw shapes. Collectively, these four PCs account for approximately 89% of the variation in shape, with each contributing more than 5% of the variation.

Principal Component	Variance Contributed	Cumulative Proportion
GM PC1	0.57	0.57
GM PC2	0.16	0.73
GM PC3	0.11	0.84
GM PC4	0.05	0.89

4. Discussion

Numerous studies of amniotes, particularly birds and squamates, have examined variation in claw shape in an ecomorphological framework and found that claw shape varies with microhabitat use, suggesting an interaction between claw shape, function, and environment (Crandell et al., 2014; D'Amore et al., 2018; Feduccia, 1993; Teixeira-Filho et al., 2001; Thomson and Motani, 2021; Tulli et al., 2009; Yuan et al., 2019). Most of these studies, however, did not examine functional morphological associations empirically. Instead, most authors cited a single

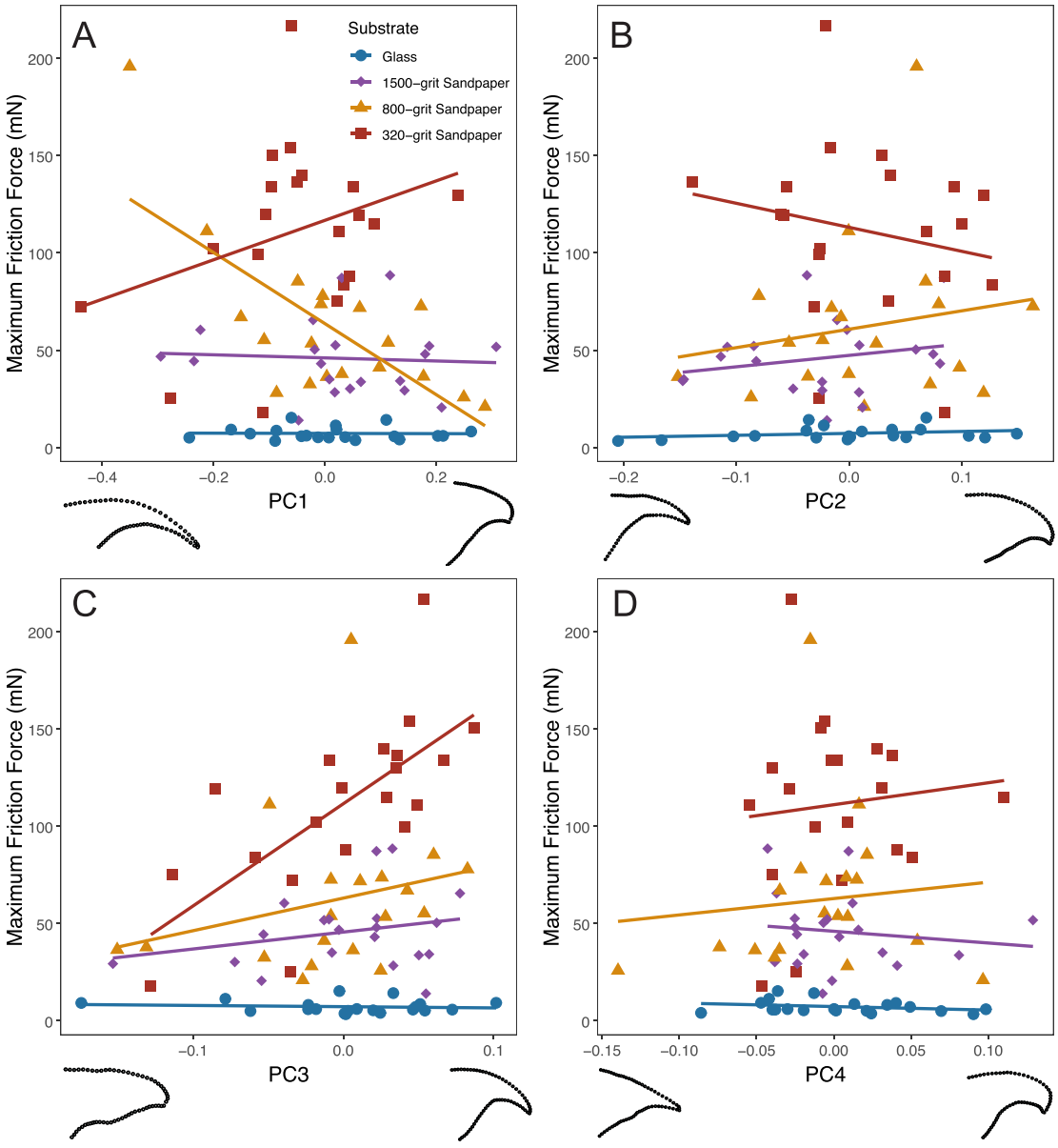

Fig. 4. Maximum friction force induced on each of the four substrates as a function of the four principal component axes of *Anolis equestris* claw morphology in the main sample as measured by semilandmarks. The main sample includes both unmodified and modified (shape manually altered with rotary tool) claws. Some claws were modified to sample a greater variety of potential claw shapes. The x-axis of each graph represents the range of variation of each principal component, with the extreme values represented by the schematics below the graph. Panels A, B, C, and D contain data for GM PC1, GM PC2, GM PC3, and GM PC4, respectively. Only two regression lines are significant: 800-grit sandpaper for GM PC1 (R^2 =0.51, $p < 0.001$) and 320-grit sandpaper for GM PC3 (R^2 =0.49, $p < 0.001$). Friction force increases with more negative values of GM PC1 (longer claws with smaller tips) and more positive values of GM PC3 (smaller opening angles of the ventral curve).

Table 3
Statistical results for the effect of each principal component (derived from geometric morphometric data – GM) on maximum friction force production on the four substrates used on the main sample of *Anolis equestris* claws. The main sample includes both unmodified and modified (shape manually altered with rotary tool) claws. Some claws were modified to sample a greater variety of potential claw shapes. The four principal components in this table were derived from semilandmark data. Significant values are denoted with asterisks. F-values and degrees of freedom are reported in SI Table 6.

	GM Principal Component 1		GM Principal Component 2		GM Principal Component 3		GM Principal Component 4	
	R^2	*p*	R^2	*p*	R^2	*p*	R^2	*p*
Glass	$5.0 * 10^{-4}$	0.92	0.07	0.25	0.01	0.63	0.07	0.25
1500-grit sandpaper	$3.9 * 10^{-3}$	0.79	0.05	0.36	0.06	0.29	0.02	0.58
800-grit sandpaper	0.51 *	< 0.001 *	0.03	0.45	0.06	0.31	0.01	0.67
320-grit sandpaper	0.11	0.16	0.04	0.40	0.49 *	< 0.001 *	0.01	0.67

Table 4
Statistical results for the effect of each principal component (as calculated by univariate measurements – UM) on maximum friction force production on the four substrates used in the main sample. The main sample includes both unmodified and modified (shape manually altered with rotary tool) claws. Some claws were modified to sample a greater variety of potential claw shapes. The two principal components in this table were derived from univariate data on claw length, depth, and curvature in *Anolis equestris*. Significant values are denoted with asterisks. F-values and degrees of freedom are reported in SI Table 7.

	UM Principal Component 1		UM Principal Component 2	
	R^2	*p*	R^2	*p*
Glass	$8.00 * 10^{-3}$	0.71	0.06	0.30
1500-grit sandpaper	0.07	0.28	$5.41 * 10^{-4}$	0.92
800-grit sandpaper	0.01	0.63	0.13	0.14
320-grit sandpaper	0.24	0.03 *	$9.12 * 10^{-4}$	0.90

Table 5
Loadings of the univariate measures (UM) for Principal Components 1 and 2 of claw shape in *Anolis equestris*. Measurements are from the main sample, which includes both unmodified and modified (shape manually altered with rotary tool) claws. Some claws were modified to sample a greater variety of potential claw shapes.

Univariate Measure	UM Principal Component 1	UM Principal Component 2
Curvature	0.22	0.97
Length	0.90	0.001
Depth	0.88	-0.25

previous study that assayed clinging ability across multiple species of lizards, including several species that possess adhesive toe pads. These investigations thus render it difficult to ascertain whether claw shape influences clinging ability directly, indirectly via interaction with adhesive toe pads, or a combination of these. Here we isolated claws from the digits of *Anolis equestris*, measured natural and induced morphological variation using geometric morphometrics, and assayed frictional performance on a variety of substrates that varied in surface roughness to, for the first time, make explicit connections between claw shape and function in isolation from the rest of the digit.

We expected the three sandpapers used in this study to comprise a gradient from smoothest to roughest based on commonly used surface roughness parameters in studies of organismal attachment, such as mean arithmetic height (R_a) and root mean square (RMS) height (R_q) (Bullock and Federle, 2011; Scholz et al., 2010). Although 320-grit sandpaper had the greatest R_a and R_q, the 1500-grit sandpaper and 800-grit sandpaper were nearly identical in terms of these values. Despite this apparent similarity, claws interact with these surfaces differently. Fig. 3 shows different trends in peak friction force as a function of substrate, with it being generally greater on the 800-grit sandpaper compared to the 1500-grit sandpaper. It is critical to recognize that despite the use and adoption of single parameters to describe the "roughness of a surface" (e.g., R_a and R_q), surfaces with similar parameters can nonetheless vary in other ways (e.g., $R_{\Delta q}$, R_{sm}, etc.) that impact macroscopic phenomena (e.g., friction, adhesion, wetting) (Jacobs et al., 2017; Niewiarowski et al., 2019; Palecek et al., 2022). Indeed, other qualities of surface roughness must be governing the differential performance of claws on these substrates.

Many studies examining the attachment performance of animal claws on rough substrates model asperities of rough surfaces as a series of hemispheres that differ in diameter (Dai et al., 2002; Pattrick et al., 2018). Correspondingly, these studies often relate claw performance to surface roughness parameters that describe asperity height (or diameter in the case of hemispherical asperities), such as R_a or R_q. Dai et al. (2002), for example, studied the friction forces of the tarsal claw of the sun beetle (*Pachnoda marginata*) on a variety of rough substrates and concluded that mechanical interlocking of claws is only possible when the diameter of the claw tip is smaller than asperity height. Although asperity height may be involved in the process of mechanical interlocking to some extent, it is likely that the spacing between asperities is more important for the induction of mechanical interlocking. If the distance between two adjacent asperities is much smaller than the diameter of the claw tip, the claw will be unable to penetrate the surface depression and will thus only contact some fraction of the exposed asperities. In contrast, if the distance between two asperities is sufficiently greater than the diameter of the claw tip then the claw should be able to penetrate deeper into the space and permit effective interlocking between the two asperities. In the case of softer substrates, the shape of the tip may be important for perforation of the surface as well. We calculated the mean spacing of the asperities of our four test substrates

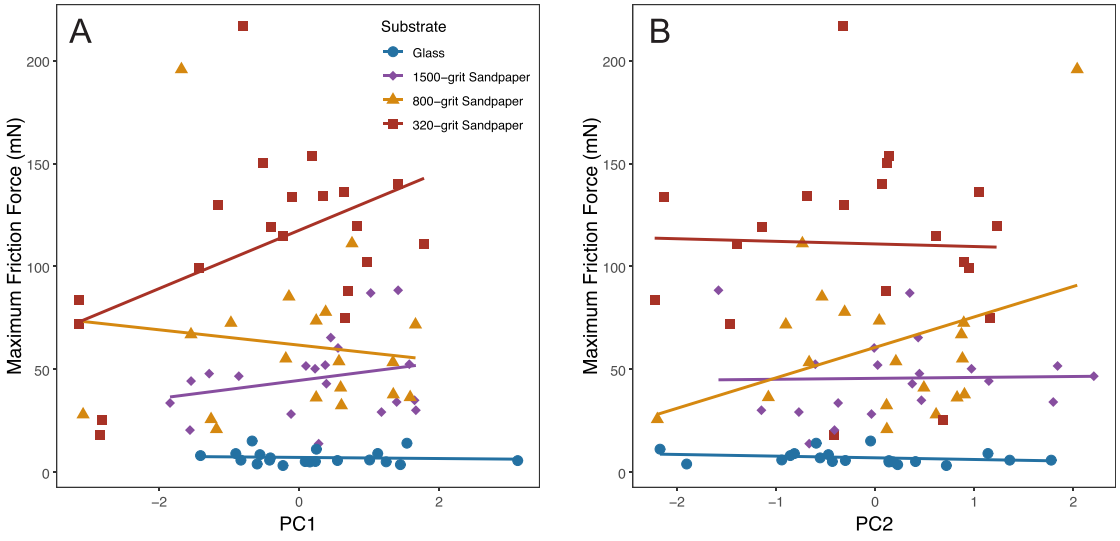

Fig. 5. Maximum friction force induced on each of the four substrates as a function of the principal component axes of univariate *Anolis equestris* claw morphology. These data are drawn from the main sample of claws and includes both unmodified and modified (shape manually altered with rotary tool) claws. Some claws were modified to sample a greater variety of potential claw shapes. The x-axis of each graph represents the range of variation of each principal component. Panels A and B contain data for UM PC1 and UM PC2, respectively. Only one regression line is significant: 320-grit sandpaper for UM PC1 (R^2 =0.24, $p = 0.03$). Friction force increases with more positive values of UM PC1 (longer and deeper claws).

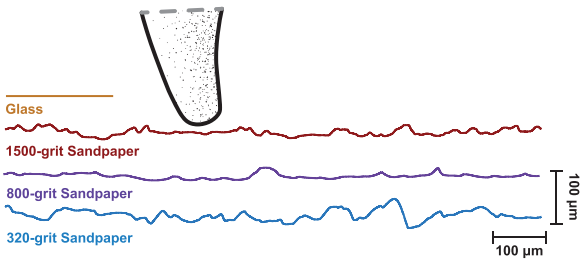

Fig. 6. Scaled depictions of the interactions between the claw tip and our various substrates. Profiles were obtained via stylus profilometry, and the claw tip schematic was created from a high-magnification optical microscopy image of a natural, representative *Anolis equestris* claw. Images show the claw tip interacting with glass, 1500-grit sandpaper, 800-grit sandpaper, and 320-grit sandpaper. The vertical and horizontal scale bars are 100 µm.

(Table 1) and found that spacing between asperities increases with increasing grit size. If we represent one of our light microscopic images of an exemplar, unmodified claw of *A. equestris* as a 2-dimensional scaled schematic, we can align this with representative surface profile scans of our four substrates to visually model this claw's interaction with each of our substrates (Fig. 6) and explain the trends we observed in friction as a function of substrate (Fig. 3). As expected, there are no perceptible asperities on the glass surface relative to claw tip diameter; as such, friction is limited to the interaction between the claw tip and the relatively smooth glass surface. At the other extreme, 320-grit sandpaper has large inter-asperity distances suggesting that mechanical interlocking can occur. The 800-grit sandpaper profile possesses fewer large asperities compared to the 320-grit sandpaper, but still has very large inter-asperity distances, suggesting that mechanical interlocking can occur, although fewer such asperities are available. The 1500-grit sandpaper profile, on the other hand, is comprised of many smaller asperities with inter-asperity distances that are most often smaller than the diameter of the claw's tip, suggesting that mechanical interlocking is less likely to occur with its surface. Our approach here of combining statistical descriptors of surface roughness, visual modeling of a claw-substrate interaction (Fig. 6), and measurement of *ex situ* frictional interactions of claws on rough substrates supports the hypothesis that the spacing between asperities, an often-overlooked parameter of surface roughness, is an important predictor of claw performance. Of course, the sample of surface profiles presented here certainly does not comprise a representative sampling of real surfaces that a free-ranging, clawed lizard may encounter and may, instead, impose an artificial lower limit on surface roughness. Furthermore, the surfaces that lizards interact with are three-dimensional and complex and may therefore possess qualities not characterized in most studies that are critical for claw function. For example, few studies have considered three-dimensional surface roughness parameters (besides areal equivalents of R_a and R_q) in relation to claw form and function. It is likely that three-dimensional asperity dimensions (height and diameter) and spacing interact with claw shape to influence friction forces. Future work may investigate these topics further with natural surfaces exploited by lizards in their natural habitats and area-based surface roughness measurement techniques.

After quantifying multivariate claw shape using geometric morphometrics (Tinius and Russell, 2017), we found that several aspects of claw shape correlate with friction, but that these correlations were dependent upon substrate. On 800-grit sandpaper, longer claws with shallower bases, smaller opening angles, and a greater degree of taper (GM PC1) induced significantly greater friction forces than deeper and shorter claws with less taper (Fig. 4a). On 320-grit sandpaper, claws with a relatively tighter inner curve and greater degree of taper (GM PC3) performed significantly better than those with relatively looser inner curves and less taper (Fig. 4c). Here, claws described as having greater taper are more consistent along their length in their change in height. For example, the PC1 shape minimum decreases relatively consistently in height from base to tip, while the PC1 shape maximum retains a greater height and then ends abruptly (Fig. 4a). The geometric morphometric methods employed here do not directly provide information about claw tip diameter, another morphological parameter of claws thought to impact frictional interactions with rough substrates, because semilandmarks are only placed on the dorsal and ventral curves of claws. Interestingly, however, independent measurements of claw tip diameter, measured as the length of the flattened segment connecting the dorsal and ventral curves of the claw at the distal end, vary significantly and positively with the three geometric morphometric principal component axes (GM PC1 – GM PC3) that explain variation in degree of claw tapering (all $p < 0.01$; Fig. S2). These findings indicate that our geometric morphometric methods also indirectly describe variation in claw tip diameter because of its positive relationship with claw tapering. As such, our results suggest that claws with greater degrees of taper and smaller tip diameters induced the greatest friction forces on the 320-grit and 800-grit sandpapers, indicating that the effectiveness of mechanical interlocking on these surfaces is largely dependent upon these variables. On the roughest of our substrates, the opening angle of the claws significantly impacted friction, with hook-like claws inducing greater friction than straighter claws (Zani, 2000). Surprisingly, we did not observe this dependence on the 800-grit sandpaper. This latter surface had much lower root mean square slope ($R_{\Delta q}$) values than the other two sandpaper substrates, indicating that the slopes of asperities present on the 800-grit sandpaper are much shallower than those of the other sandpapers. Claws that are more hook-like are more effective at re-orienting force onto the vertical slope of asperities than are straighter claws, which likely improves the efficacy of mechanical interlocking (Cartmill, 1974; Tulli et al., 2012). If the slopes of asperities, however, are relatively shallow (as is the case for the 800-grit sandpaper), increased claw curvature appears not to provide an advantage in terms of mechanical interlocking.

It is not clear why friction is dependent on claw length and depth on the 800-grit sandpaper substrate, with longer, shallower claws producing greater friction than shorter, deeper ones. If modeled as a cantilever beam, a long, shallow claw is likely to have a lower bending stiffness than a shorter, deeper claw, yet a claw with lower stiffness would likely be disadvantageous for mechanical interlocking because the claw would be more likely to deform under stress and slip off of an asperity on the substrate (Asbeck et al., 2006; Dai et al., 2002). Future work may consider generating physical and theoretical models of claws and surfaces they interact with to examine how the fundamental parameters observed here and in other work relate to their mechanical and frictional properties.

Friction on the glass substrate and 1500-grit sandpaper did not vary significantly with any multivariate representation of claw shape. Given our discussion above, this result is not surprising because the inter-asperity distances of these surfaces are generally too small to promote mechanical interlocking and thus the interaction between the claw tip and the surface is largely responsible for the friction forces observed. If we use the average maximum friction force on these substrates and multiply it by 20, we can estimate the total friction an animal could generate on either substrate. Not surprisingly, an animal could only generate approximately 0.18 N of friction on glass, which is insufficient to support the average body mass of the anoles used in this study (70.3 $\pm$ 10.7 g). Conversely, an animal could generate approximately 1.14 N of friction on 1500-grit sandpaper, which is nearly double the force required to support the average body mass of the anoles used in this study. This suggests that mechanical interlocking is not necessary for stationary attachment on rough substrates, but that it is likely important for effective locomotion on vertical substrates where reaction forces can be double the animal's body mass or more (e.g., Autumn et al., 2006). Of course, anoles, like many geckos, possess adhesive toe pads that will likely contribute to the total friction force generated by the animal during locomotion (Naylor and Higham, 2019). Future work should

investigate the individual and combined roles of claws during stationary attachment and adhesive locomotion on vertical substrates and how, or if, this depends on substrate roughness.

Our findings conflict with those of Zani (2000), who demonstrated a positive correlation between claw curvature and clinging force on smooth acrylic and a positive correlation between claw depth and clinging force on rough surfaces. One explanation for this discrepancy is the inclusion of adhesive toe pads in Zani's investigation and the complete isolation of the claw in ours. The findings of previous studies measuring clinging ability before and after experimental claw removal suggest that the claw does not significantly influence the ability of adhesive toe pads to effectively attach to a smooth surface (Garner et al., 2017; Naylor and Higham, 2019). Our study found that claw shape does not significantly impact friction on a smooth substrate in any manner, suggesting that the relationship between claw curvature and clinging ability on a smooth substrate has no functional relevance. Arboreal *Anolis* tend to have claws with tighter curvature and relatively larger adhesive toe pads than those that are more terrestrial (Elstrott and Irschick, 2004; Yuan et al., 2019). Not surprisingly, size-corrected clinging ability scales positively with size-corrected adhesive toe pad area (Elstrott and Irschick, 2004). Therefore, the positive relationship between claw curvature and clinging ability may simply be a consequence of arboreal anoles possessing relatively larger adhesive pads that can induce greater attachment on smooth substrates. Future work characterizing the variation in natural substrate surface properties is critical for furthering our understanding of the relationships between form, function, and environment in these systems (Niewiarowski et al., 2016; Niewiarowski et al., 2019).

We did, however, corroborate the significance of claw depth with friction on rougher surfaces. In previous *in vivo* work, a deeper claw base results in a longer in-lever for the flexor tendon, which provides greater forces with similar muscular input (Fig. 1) (Cartmill, 1985; Russell, 1975; Thomson and Motani, 2021; Zani, 2000). We expect claw depth to significantly improve friction on rough substrates *in vivo*, as has been demonstrated on multiple occasions (Tulli et al., 2012; Zani, 2000). However, in our study muscular input was entirely removed and the angle of the claw was fixed. There is evidence that claws with deeper bases are stiffer and induce higher forces as a result (Crandell et al., 2014; D'Amore et al., 2018; Falvey et al., 2020). This may explain why our study obtained similar results to previous studies through a different combination of mechanisms. However, bending stiffness will also depend on the thickness of the claw along its proximodistal axis and few studies have examined the functional morphology of claws in three dimensions (Tsang et al., 2019), nor have robust mechanical models been tested across vertebrates to investigate this (but see Dai et al., 2002).

5. Conclusions

Investigating how the form of a biomechanical system physically influences function is critical for a holistic understanding of the connections between form, function, and environment. Here we examined the influence of claw shape on friction *ex vivo* and found that although claw morphology does not affect friction on smooth surfaces in any manner, it is critical to the achievement of mechanical interlocking on rough surfaces. Specifically, our findings suggest that claw shape only influences friction when mechanical interlocking is possible, which is governed by the distance between asperities relative to the diameter of the claw's tip. Furthermore, we found that claw tip diameter and the degree of tapering were the most consistent predictors of friction on substrates on which mechanical interlocking was possible: narrower claw tips induced greater friction than wider ones. We also found that other claw parameters such as tightness of curvature, length, and depth influence friction, but that these relationships are dependent on the substrate's surface roughness. We estimated that frictional interactions without mechanical interlocking are sufficient to permit whole animal stationary attachment on certain rough substrates, but our findings suggest that mechanical interlocking is critical for supporting effective vertical locomotion when claws alone are the attachment devices. Although this study analyzed claw shape in isolation from the rest of the animal, contributions from other attachment organs, such as adhesive toe pads, are certainly important factors in whole animal attachment performance. Clearly, additional work is needed for a holistic understanding of the effects of, and interactions among, claw form, function, and environment on organismal attachment.

Funding

A.P.R. acknowledges financial support from a Natural Science and Engineering Research Council of Canada Discovery Grant (9745–2008). A.D. acknowledges financial support from the National Science Foundation (NSF DMR-1610483).

Declaration of Competing Interest

The authors declare that they have no known competing financial interests or personal relationships that could have appeared to influence the work reported in this paper.

Data availability

All data from this study are available at figshare at the following link: https://doi.org/10.6084/m9.figshare.19606372.

Acknowledgments

We would like to thank Dr. Saranshu Singla and the Dhinojwala Research Group for assistance with the friction cell and Dr. Jiangsheng Feng for assistance with stylus profilometry measurements. We would also like to thank Dr. Natasha S. Vitek and the Gecko Adhesion Research Group for providing helpful feedback and discussion. We also thank two anonymous reviewers for their helpful and insightful commentary on this manuscript.

Appendix A. Supporting information

Supplementary data associated with this article can be found in the online version at doi:10.1016/j.zool.2023.126078.

References

Adams, D., Collyer, M., Kaliontzopoulou, A. and Sherratt, E. (2017). geomorph: Geometric morphometric analyses of 2D/3D landmark data.

Asbeck, A.T., Kim, S., Cutkosky, M.R., Provancher, W.R., Lanzetta, M., 2006. Scaling hard vertical surfaces with compliant microspine arrays. Int. J. Robot. Res. 25, 1165–1179.

Autumn, K., Peattie, A.M., 2002. Mechanisms of adhesion in Geckos. Integr. Comp. Biol. 42, 1081–1090.

Autumn, K., Hsieh, S.T., Dudek, D.M., Chen, J., Chitaphan, C., Full, R.J., 2006. Dynamics of geckos running vertically. J. Exp. Biol. 209, 260–272.

Bloch, N., Irschick, D.J., 2005. Toe-clipping dramatically reduces clinging performance in a pad-bearing lizard (Anolis carolinensis). hpet 39, 288–293.

Bullock, J.M.R., Federle, W., 2011. The effect of surface roughness on claw and adhesive hair performance in the dock beetle Gastrophysa viridula. Insect Sci. 18, 298–304.

Cartmill, M., 1974. Pads and Claws in Arboreal Locomotion. Primate Locomotion. Academic Press, Inc, New York, New York, pp. 45–83.

Cartmill, M., 1985. Climbing. Functional vertebrate morphology. Harvard University Press, Cambridge, USA, pp. 73–88.

Crandell, K.E., Herrel, A., Sasa, M., Losos, J.B., Autumn, K., 2014. Stick or grip? Co-evolution of adhesive toepads and claws in Anolis lizards. Zoology 117, 363–369.

Dai, Z., Gorb, S., Schwarz, U., 2002. Roughness-dependent friction force of the tarsal claw system in the beetle Pachnoda marginata (Coleoptera, Scarabaeidae). J. Exp. Biol. 205, 2479–2488.

D'Amore, D.C., Clulow, S., Doody, J.S., Rhind, D., McHenry, C.R., 2018. Claw morphometrics in monitor lizards: Variable substrate and habitat use correlate to shape diversity within a predator guild. Ecol. Evol. 8, 6766–6778.

Elstrott, J., Irschick, D.J., 2004. Evolutionary correlations among morphology, habitat use and clinging performance in Caribbean Anolis lizards: COMPARATIVE CLINGING. Biol. J. Linn. Soc. 83, 389–398.

Falvey, C.H., Aviles-Rodriguez, K.J., Hagey, T.J., Winchell, K.M., 2020. The finer points of urban adaptation: intraspecific variation in lizard claw morphology. Biol. J. Linn. Soc. blaa123.
Feduccia, A., 1993. Evidence from claw geometry indicating arboreal habits of archaeopteryx. Science 259, 790–793.
Garner, A.M., Lopez, S.M., Niewiarowski, P.H., 2017. Brown anole (Anolis sagrei) adhesive forces remain unaffected by partial claw clipping. Acta Herpetol. 12, 133–137.
Garner, A.M., Wilson, M.C., Wright, C., Russell, A.P., Niewiarowski, P.H., Dhinojwala, A., 2021. The same but different: setal arrays of anoles and geckos indicate alternative approaches to achieving similar adhesive effectiveness. J. Anat. 238, 1143–1155.
Gunz, P., Mitteroecker, P., 2013. Semilandmarks: a method for quantifying curves and surfaces. Hystrix 24.
Jacobs, T.D.B., Junge, T., Pastewka, L., 2017. Quantitative characterization of surface topography using spectral analysis. Surf. Topogr.: Metrol. Prop. 5, 013001.
Klingenberg, C.P., 2016. Size, shape, and form: concepts of allometry in geometric morphometrics. Dev. Genes Evol. 226, 113–137.
Maderson, P.F.A., 1964. Keratinized epidermal derivatives as an aid to climbing in Gekkonid lizards. Nature 203, 780–781.
Naylor, E.R., Higham, T.E., 2019. Attachment beyond the adhesive system: the contribution of claws to Gecko clinging and locomotion. Integr. Comp. Biol. 59, 168–181.
Niewiarowski, P.H., Stark, A.Y., Dhinojwala, A., 2016. Sticking to the story: outstanding challenges in gecko-inspired adhesives. J. Exp. Biol. 219, 912–919.
Niewiarowski, P.H., Dhinojwala, A., Garner, A.M., 2019. A physical model approach to gecko adhesion opportunity and constraint: how rough could it be? Integr. Comp. Biol. 59, 203–213.
Palecek, A.M., Garner, A.M., Klittich, M.R., Stark, A.Y., Scherger, J.D., Bernard, C., Niewiarowski, P.H., Dhinojwala, A., 2022. An investigation of gecko attachment on wet and rough substrates leads to the application of surface roughness power spectral density analysis. Sci. Rep. 12, 11556.
Pattrick, J.G., Labonte, D., Federle, W., 2018. Scaling of claw sharpness: mechanical constraints reduce attachment performance in larger insects. J. Exp. Biol. 221, jeb188391.
Rohlf, F.J. (2018). tpsDig2 version 2.31.
Russell, A.P., 1975. A contribution to the functional analysis of the foot of the Tokay, Gekko gecko (Reptilia: Gekkonidae). J. Zool. 176, 437–476.
Russell, A.P., Johnson, M.K., 2007. Real-world challenges to, and capabilities of, the gekkotan adhesive system: contrasting the rough and the smooth. Can. J. Zool. 85, 1228–1238.
Russell, A.P., Johnson, M.K., 2014. Between a rock and a soft place: microtopography of the locomotor substrate and the morphology of the setal fields of Namibian day geckos (Gekkota: Gekkonidae: Rhoptropus). Acta Zool. 95, 299–318.
Scholz, I., Bückins, M., Dolge, L., Erlinghagen, T., Weth, A., Hischen, F., Mayer, J., Hoffmann, S., Riederer, M., Riedel, M., et al., 2010. Slippery surfaces of pitcher plants: nepenthes wax crystals minimize insect attachment via microscopic surface roughness. J. Exp. Biol. 213, 1115–1125.
Teixeira-Filho, P., Rocha-Barbosa, O., Paes, V., Carvalho Ribas, S., de Almeida, J.R., 2001. Ecomorphological relationships in six lizard species of Restinga da Barra de Marica, Rio de Janeiro, Brazil. Rev. Chil. Anat. 19.
Thomson, T.J., Motani, R., 2021. Functional morphology of vertebrate claws investigated using functionally based categories and multiple morphological metrics. J. Morphol. 282, 449–471.
Tinius, A., Russell, A.P., 2017. Points on the curve: an analysis of methods for assessing the shape of vertebrate claws. J. Morphol. 278, 150–169.
Tsang, L.R., Wilson, L.A.B., Ledogar, J., Wroe, S., Attard, M., Sansalone, G., 2019. Raptor talon shape and biomechanical performance are controlled by relative prey size but not by allometry. Sci. Rep. 9, 7076.
Tulli, M.J., Cruz, F.B., Herrel, A., Vanhooydonck, B., Abdala, V., 2009. The interplay between claw morphology and microhabitat use in neotropical iguanian lizards. Zoology 112, 379–392.
Tulli, M.J., Herrel, A., Vanhooydonck, B., Abdala, V., 2012. Is phylogeny driving tendon length in lizards? Acta Zool. 93, 319–329.
Virtanen, P., Gommers, R., Oliphant, T.E., Haberland, M., Reddy, T., Cournapeau, D., Burovski, E., Peterson, P., Weckesser, W., Bright, J., et al., 2020. SciPy 1.0: fundamental algorithms for scientific computing in Python. Nat. Methods 17, 261–272.
Wang, M., Kornblau, S.M., Coombes, K.R., 2018. Decomposing the apoptosis pathway into biologically interpretable Principal components. Cancer Inf. 17, 1176935118771082.
Yuan, M.L., Wake, M.H., Wang, I.J., 2019. Phenotypic integration between claw and toepad traits promotes microhabitat specialization in the Anolis adaptive radiation. Evolution 73, 231–244.
Zani, P., 2000. The comparative evolution of lizard claw and toe morphology and clinging performance. J. Evol. Biol. 13, 316–325.